Repeated Transcranial Photobiomodulation with Light Emitting Diodes Improves Psychomotor Vigilance and EEG Networks of the Human Brain

Akhil Chaudhari , Xinlong Wang , Anqi Wu , Hanli Liu *

Posted Date: 12 July 2023

doi: 10.20944/preprints202307.0795.v1

Keywords: Transcranial photobiomodulation, tPBM, repeated tPBM, light emitting diodes, Psychomotor Vigilance Task, PVT, Electroencephalography, EEG.

Article

Repeated Transcranial Photobiomodulation with Light Emitting Diodes Improves Psychomotor Vigilance and EEG Networks of the Human Brain

Akhil Chaudhari, Xinlong Wang, Anqi Wu and Hanli Liu *

Department of Bioengineering, University of Texas at Arlington, 500 UTA Blvd, Arlington, TX 76019, USA
* Correspondence: Hanli@uta.edu

Abstract: Transcranial photobiomodulation (tPBM) has been suggested as a non-invasive neuromodulation tool. Repetitive administration of light-emitting diode (LED)-based tPBM for several weeks significantly improved human cognition. To understand the electrophysiological effects of LED-tPBM on the human brain, we investigated alterations by repeated tPBM in vigilance performance and brain networks using electroencephalography (EEG) in healthy participants. Active and sham LED-based tPBM were administered to the right forehead of young participants twice a week for four weeks. The participants performed a psychomotor vigilance task (PVT) during each tPBM/sham experiment. A 64-electrode EEG system recorded electrophysiological signals from each participant during the first and last visits in the 4-week study. Topographical maps of EEG power enhanced by tPBM were statistically compared for the repeated tPBM effect. A new data-processing framework combining the group singular value decompensation (gSVD) with eLORETA was implemented to identify EEG brain networks. The reaction time of PVT in the tPBM-treated group was significantly improved over four weeks compared to that in the sham group. We observed acute increases in EEG delta and alpha powers during 10-min LED-tPBM while the participants performed the PVT task. We also found that theta, beta, and gamma EEG powers significantly increased globally after four weeks of LED-tPBM. Combining gSVD with eLORETA enabled us to identify EEG brain networks and the corresponding network power changes by repeated 4-week tPBM. This study clearly demonstrated that 4-week prefrontal LED-tPBM can neuromodulate several key EEG networks, implying a possible causal effect between modulated brain networks and improved psychomotor vigilance outcomes.

Keywords: transcranial photobiomodulation; tPBM; repeated tPBM; light emitting diodes; psychomotor vigilance task; PVT; Electroencephalography; EEG

1. Introduction

Transcranial photobiomodulation (tPBM) is a new, noninvasive intervention tool that involves delivering near-infrared (NIR) light in the range of 800-1070 nm with laser or light-emitting diodes (LEDs) to the human head [1–3]. This type of light can safely reach the cortical and subcortical regions and stimulate neuronal function as a reparative and protective tool in a noninvasive manner [4–6]. The underlying principle of tPBM is based on mitochondrial light absorption by cytochrome c oxidase (CCO), which plays a key role in neuronal oxygen utilization for energy metabolism [3,7,8]. This photonics-bioenergetics mechanism results in unique metabolic effects on the living brain, with benefits for neural enhancement and neuroprotection [9,10]. Numerous recent studies have reported that tPBM has facilitated effective treatment of neurological disorders [11–16], including Alzheimer's disease (AD) and dementia [17–22], as reviewed in the literature [23–25]. The benefits of tPBM as an intervention strategy include its low cost, compactness, self-administration, and routine use in repeated care.

For tPBM to become an effective therapeutic tool, it is necessary to understand its underlying neurophysiological mechanisms. It is accepted that the oxidized form of CCO (oxi-CCO) plays a key role in the utilization of neuronal oxygen for energy metabolism [11]. This CCO-driven mechanism of tPBM was experimentally demonstrated by Wang et al. [26–28], who showed that tPBM at 1064

 doi:10.20944/preprints202307.0795.v1

nm can noninvasively stimulate mitochondrial metabolism in living human tissues. This set of experimental observations is supported by reproducible results [29] and another independent human study [30].

However, studies on tPBM-induced electrophysiological effects in the human brain are limited, with only a few publications [17,31–34] besides ours [26,35,36] in the last 4-5 years. All these studies reported acute alterations in electroencephalogram (EEG) power by tPBM compared to sham stimulation, without any repeated tPBM treatment. Furthermore, the protocol used to achieve significant improvement in cognition in older adults with or without AD required daily tPBM administration over one or two months, respectively [18,19]. Such critical daily administration of tPBM appears to be key to success and thus necessitates an understanding of the repeated effects of tPBM on the human brain. In addition, while a few articles have reported cognitive improvements by acute tPBM in healthy humans [37,38], no report has been found in the literature on repeated vigilance improvement along with their electrophysiological effects after repeated tPBM administration for weeks in healthy participants.

The psychomotor vigilance task (PVT) is a sustained attention game that has been used to measure the speed of response to a visual stimulus and has been recognized as an effective tool for evaluating sustained attentional performance [39]. Thus, PVT has been routinely used to examine and demonstrate significant acute improvements in attention after laser stimulation [37,38,40]. Vargas et al. also showed an improvement in the reaction time over five weeks under laser stimulation in older adults [32].

In this study, we designed and conducted the first sham-controlled human study to demonstrate that 4-week repeated tPBM by a cluster of LEDs (LED-tPBM) enabled significant improvement in human vigilance performance in healthy young adults. Moreover, we recorded acute and repeated electrophysiological effects using a 64-channel EEG during the first and last sessions of the 4-week tPBM or sham experiments. Consequently, we propose three hypotheses that will be proven at the end of this study. First, repeated LED-tPBM of the right forehead of healthy subjects significantly improved vigilance. Second, acute LED-tPBM significantly increased topographical EEG delta and alpha powers. Third, the four-week repeated LED-tPBM enhanced several brain network strengths (such as default mode, executive control, and frontal parietal networks) in all five EEG frequency bands. Specifically, we utilized frequency-domain analysis to quantify channel-wise EEG power alterations by acute LED-tPBM to support Hypothesis 2 [41], and a newly developed inverse algorithm [36] to demonstrate that repeated tPBM significantly enhanced key EEG brain networks to support Hypothesis 3. In conclusion, this study revealed an objective association between improved vigilance and tPBM-modulated brain networks in healthy humans, providing evidence that tPBM is a potential intervention tool for enhancement of human cognition in healthy humans and for effective treatment of neurological diseases, including AD.

2. Materials and Methods

2.1 Study participants

This study employed a between-groups experimental design. Twenty-two healthy volunteers (seven males and 15 females; mean age = 26 ± 5 years) were recruited from the university community. Each subject was randomly assigned to either the active or sham group; therefore, there were 11 participants in each of the tPBM and sham groups. All participants had normal or corrected-to-normal vision and were neurologically and psychologically healthy. Subjects were excluded if they were younger than 18 years of age, currently pregnant (during the recruitment), had a neurological disease, diabetes, psychiatric illness, had any tattoos on the head and face, or had caffeine consumed within 3 hours before the experiment. PVT is believed to be sensitive to caffeine [42]. The study protocol complied with all applicable federal guidelines and was approved by the Institutional Review Board (IRB) of the University of Texas at Arlington. Written informed consent for the sham-controlled LED-tPBM experiment was obtained from each participant before each set of experiments. All participants were compensated for their participation after their last visit.

Preprints (www.preprints.org) | NOT PEER-REVIEWED | Posted: 12 July 2023 doi:10.20944/preprints202307.0795.v1

2.2. Experimental Setup and protocol for LED-tPBM

LED-tPBM stimulation was delivered to the right forehead using a continuous-wave (CW) LED handheld probe (Thor-LX2, THOR Photomedicine Inc, Maryland, USA; Figure 1(a)). Table 1 lists several key parameters of the LED-tPBM setup. Accordingly, the average irradiance per wavelength was 30 mW/cm^2; thus, the maximal optical dose or fluence delivered to the human forehead by tPBM over 10 min was approximately equal to =30 mJ/s/cm^2 × 32 cm^2 × 10 min x60 s/min = 576 J. On the other hand, the power used for sham was set to be 0.0 W. On the other hand, the power used for sham was set to be 0.0 W.

Table 1. LED-tPBM parameters used in the study.

Wavelength	660, 810 nm
Operation model	CW
Aperture diameter	6.4 cm
Total aperture area	32 cm^2
Total number of LED emitters	69
Averaged irradiance	~30 mW/cm^2

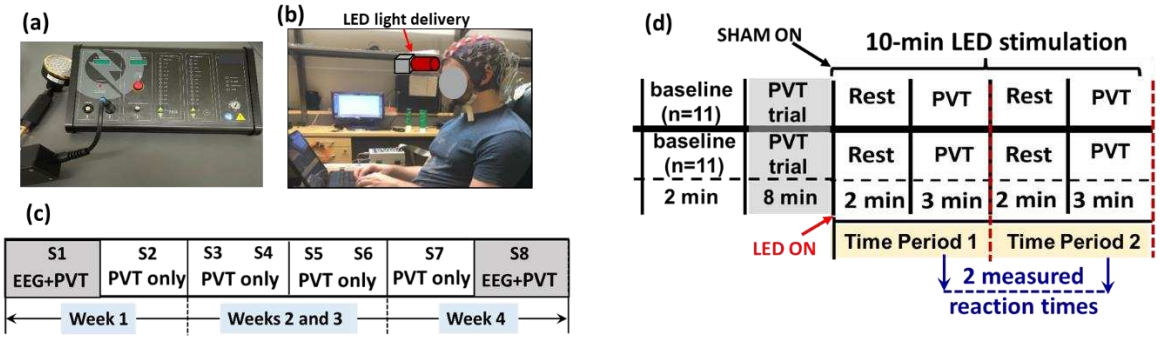

Figure 1. A photograph of (a) the LED-tPBM unit used for the study and (b) a participant wearing an EEG cap and performing PVT while the LED light was delivered to the right forehead. (c) Diagram of the experimental protocol, showing a total of eight sessions of the experiment, S1 to S8, over four weeks. EEG measurements were taken concurrently while the participants performed PVT only in S1 of week 1 and S8 of week 4. (d) A schematic illustration for each of the 8 sessions. This between-group experimental design included 11 subjects randomly assigned to either the active or the sham group. The entire experiment lasted for 20 min. During the first ten minutes, the participants in both groups were not subjected to tPBM. During the last ten minutes, the active (n=11) or sham (n=11) tPBM group was administered on the right forehead. One 2-min resting epoch and 3-min PVT epoch together consisted of one time period (TP). Participants in each group underwent TP1 and TP2 at each visit. PVT was performed twice during the 10-min tPBM period per visit. The respective reaction times were recorded twice per visit, resulting in a total of 16 reaction times measured over 4 weeks (2/visit × 2 visit/week × 4 weeks= 16).

In both the active and sham groups, the participants were seated comfortably while keeping their heads upright and wearing a pair of safety goggles (Figure 1(b)). Since the LEDs had low irradiance, the participants wearing goggles were unable to "see" or "feel" the light and thus being blind to the active or sham mode while they were told to receive active tPBM during the four-week study.

Figure 1(c) summarizes the 4-week experimental protocol. It consisted of two sessions separated by 2-3 days per week over four weeks, giving a total of eight sessions, S1 to S8. Each experimental session lasted 20 min, as shown in Figure 1(d), consisting of a 2-min baseline and 8-min trial practice

Preprints (www.preprints.org) | NOT PEER-REVIEWED | Posted: 12 July 2023 doi:10.20944/preprints202307.0795.v1

mixed with rest without any LED light exposure. The LED-tPBM was then delivered continuously for 10 min to each participant's right forehead while s/he performed two 5-min cycles (i.e., time period 1, TP1, and time period 2, TP2, as marked in Figure 1(d)) of a 2-min rest epoch and 3-min sustained attention game (PVT). During TP1 and TP2, the reaction times in response to PVT were recorded and used to assess tPBM-induced improvement in vigilance. Note that our data analysis focused only on the 10-min LED-tPBM period for both behavioral and electrophysiological measures to examine the acute effect during S1 and the repeated effect between S1 and S8.

2.3. Design of PVT and Data recording of EEG

A PVT designed by Pulsar Informatics was employed [43]. In the PVT, participants were asked to stare at a blank box at the center of a computer monitor and press the spacebar on the computer keyboard as soon as they saw a timer shown on the screen. After pressing, the timer disappeared from the monitor, followed by a returned blank box. The inter-stimulus interval time was approximately one second; each 3-min session of the PVT included 25-30 stimuli per TP. The reaction time for each stimulus was recorded for each participant. The washout period between the two visits within a week was 48 hours or longer. Furthermore, for both the sham and active tPBM groups, EEG recordings were taken continuously during the entire 20-min experiment during the first and last sessions (i.e., S1 and S8) using a 64-channel EEG system (Biosemi Instrumentation) at a data acquisition rate of 512 Hz. Before the experiment started, the participants were asked to calm themselves and pay attention to the game presented before them.

2.4 *Data analysis*

2.4.1. Behavioral data analysis

As shown in Figure 1(c), each session included two 3-min epochs of PVT with 25-30 stimuli per TP. The mean performance score for each TP was obtained by averaging the reaction times for all the stimuli per TP. This was repeated for all subjects in both the tPBM and sham groups during each visit, followed by group-level averaging of the reaction times for both groups. The time-dependent improvement in reaction time over four weeks of sham or active tPBM was evaluated for each group based on Pearson's correlation coefficient and its statistical significance. In this way, we quantified the repeated effects of LED/sham on vigilance and proved our first hypothesis.

2.4.2. EEG data preprocessing

The EEG time series were preprocessed using the EEGLAB toolbox [44,45] on the MATLAB platform. Raw EEG data taken during the 10-min LED-tPBM period (TP1 and TP2) were initially bandpass-filtered from 0.5 Hz to 70 Hz using a zero-phase Butterworth filter in MATLAB. Power line noise of 60 Hz was removed using a notch filter. The filtered data were then re-referenced to the common means across the 64 electrodes before performing Independent Component Analysis (ICA) to remove artefacts of saccades, jaw clenches, heartbeats, and eye blinks. ICA was performed using the EEGLAB function "runica". Components containing artifacts were visually inspected and removed from the data [35,46]. Next, the EEG signals were further segmented into 1 s epochs. An epoch was considered acceptable if the standard deviation of the epoch was in the range of 0.1μV up to 2 times the standard deviation of the channel. Moreover, a threshold of mean ± 4 times the standard deviation of the respective channel was applied to reject the outlier data points within each channel. Six of the participants (four from the tPBM group and two from the sham group) during the first visit and six subjects during the last visit (three from the tPBM group and three from the sham group) were removed from the study based on the previously mentioned criteria.

2.4.3. Global normalized power spectral density during 10-min tPBM/sham epoch

We temporally segmented the preprocessed data into resting and PVT phase as 2-minute and 3-minute windows, respectively. The power spectrum density (PSD) of each temporal segment was calculated using the native MATLAB function "pwelch" (sampling frequency of 512 Hz, discrete

Preprints (www.preprints.org) | NOT PEER-REVIEWED | Posted: 12 July 2023 doi:10.20944/preprints202307.0795.v1

Fourier transform points of 4 s with 50% overlap) for each electrode and subject, as shown in Step 1 in Figure 2. Pwelch resulted in a 0.25-Hz spectral resolution, ranging from 0 Hz to 128 Hz.

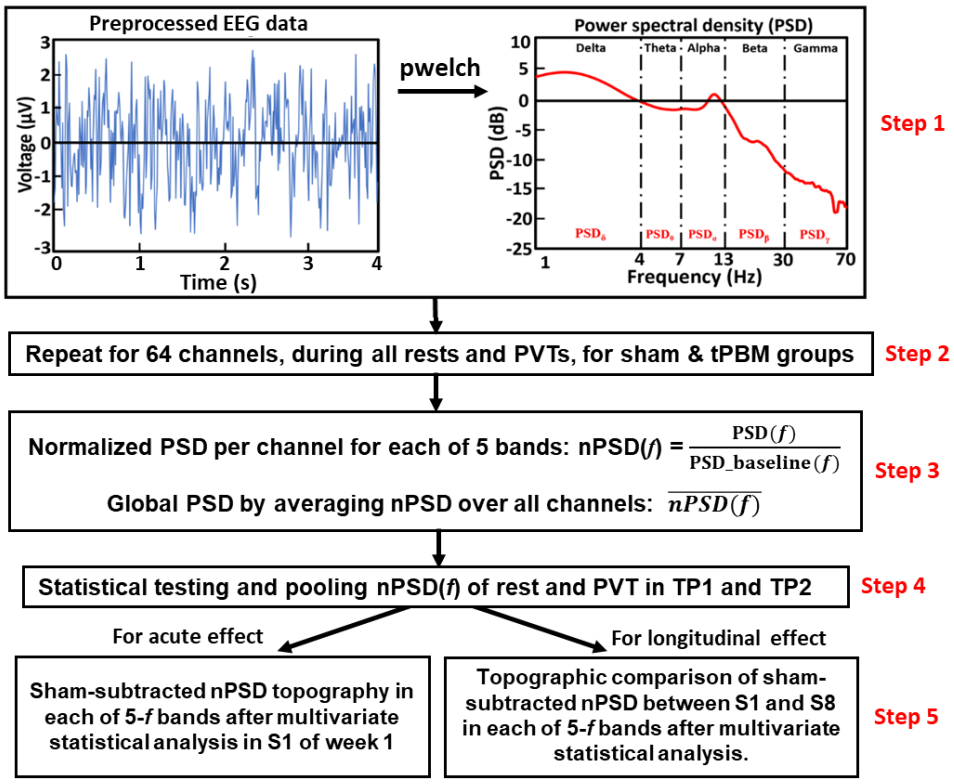

Figure 2. A flow chart showing five steps for (1) converting a time-domain series to a frequency-domain PSD, (2) repeating step 1 for all the channels, for each of the four rest/PVT epochs in two separate groups, (3) calculating channel-wise and channel-averaged (global) normalized PSD, (4) statistical testing if global normalized PSD values were significantly different between the rest and PVT epochs in each of TP1 and TP2, and (5) regrouping nPSD(*f*) to cover 5-min TP1 and TP2 for each channel and constructing sham-subtracted nPSD topography after multivariate statistical analysis for TP1 and TP2 during the 10-min tPBM/sham epoch. This analysis was performed separately to examine the acute effect during session S1 (left panel) and to determine the repeated effect of the 4-week LED-tPBM by comparing nPSD values between S1 and S8 (right panel).

For both rest and PVT epochs in each TP, the PSD values were spectrally averaged in five frequency (5-f) bands of interest, namely, delta (0.5 - 4 Hz), theta (4 - 7 Hz), alpha (7 - 13 Hz), beta (13 - 30 Hz), and gamma (30 - 70 Hz) bands, followed by normalization with respect to those in the baseline taken in the beginning of the experiment (see Figure 1(d)). This process produced a group-level normalized PSD (nPSD) at each EEG electrode in each frequency band. All nPSD values were also averaged across 64 EEG electrodes to obtain a global mean normalize PSD ($\overline{\text{nPSD}}$) in each epoch of rest and PVT in TP1 and TP2 for each participant in both the active and sham groups (Steps 2 and 3 in Figure 2). Furthermore, in TP1 and TP2, all the subjects underwent two resting and two PVT epochs. Paired t-tests were performed on paired nPSD(f) values between the 2-min rest and 3-min PVT epochs for each TP1 and TP2 using R studio [47] for both EEG data taken in S1 and S8, separately, and for each (sham and tPBM) group. This step was to examine whether we could pool the nPSD(f) values during the rest and PVT epochs together in each of TP1 and TP2 (Step 4 in Figure 2). Significant differences in nPSD at the five frequency bands were set at a significance level of $p<0.05$.

2.4.4. Topography of nPSD alterations at five frequency bands during 10-min LED-tPBM

To examine the acute effect of 10-min LED-tPBM, we generated topographic maps of nPSD at the 5-*f* bands during TP1 and TP2 in S1 of week 1. Specifically, channel-wise nPSD values at the 5-*f*

Preprints (www.preprints.org) | NOT PEER-REVIEWED | Posted: 12 July 2023 doi:10.20944/preprints202307.0795.v1

bands during Session S1 were extracted to obtain group-level averages for both the sham and tPBM groups. These averaged nPSD values were sham-subtracted to generate activation topographical maps for each TP1 and TP2 in session S1 of week 1, using the EEGLAB toolbox from the MATLAB platform. To statistically compare the differences in nPSD values topographically between the tPBM and sham groups in each of the 5-*f* bands, we performed cluster-based permutation testing [48] to solve multi-channel comparisons using the "ft_freqstatistics" function available in the Fieldtrip toolbox in MATLAB [49].

The above analysis strategy was repeated to examine the 4-week repeated effects of LED-tPBM on topographic changes in nPSD between S1 in week 1 and S8 in week 4 at all 5-*f* bands, as noted in Step 5 of Figure 2. In this case, cluster-based permutation testing examined whether the 4-week LED-tPBM could create significant alterations in EEG powers at the 5-*f* bands in certain brain regions when compared with those induced by the first 10-min tPBM in week 1.

2.4.5. The algorithm to identify EEG networks and their alterations by repeated tPBM

To further understand whether repeated LED-tPBM would have any significant impact on brain EEG networks, we applied a newly developed algorithm to identify key networks and their respective alterations by the 4-week light intervention. The new algorithm is formulated by combining group singular value decomposition (gSVD) with the exact low-resolution brain electromagnetic tomography (eLORETA). The overall process is illustrated in Figure 3.

The gSVD+eLORETA algorithm was recently introduced and published in [36] where detailed description can be found. For the convenience of readers, a brief summary of the eight steps (as listed in Figure 3) is given below, and more information on each step is provided in Section A of the Supplementary Materials.

Step 1 involved preprocessing the raw EEG data using the same procedure as described above.

Step 2 involved performing z-score transformation on each preprocessed EEG time series in a selected period to minimize inter-subject variation. This standardization step is necessary for an unbiased operation in gSVD.

Step 3 involved forming the group for computing gSVD based on the standardized EEG time series from all 32 samples of EEG measurements (n = 7 and 9 participants for the tPBM and sham groups in S1 of week 1, respectively; n = 8 and 8 for both groups in S8 of week 4, respectively). All these time series were concatenated into a single 2D matrix, M_{gSVD}. One dimension of this matrix was the concatenated time covering TP1 and TP2 in both S1 and S8 for the two groups. The other dimension was 64 channels with standardized EEG readings.

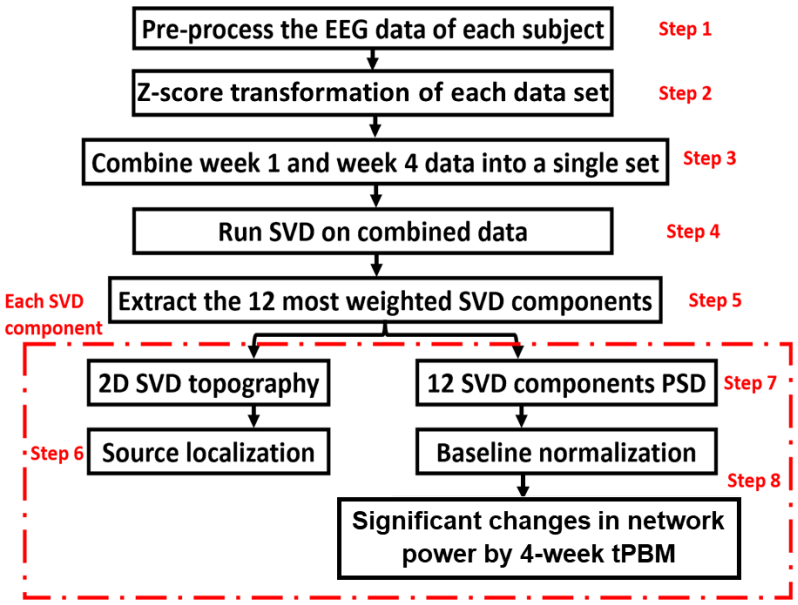

Preprints (www.preprints.org) | NOT PEER-REVIEWED | Posted: 12 July 2023 doi:10.20944/preprints202307.0795.v1

Figure 3. An EEG data processing flowchart showing eight steps to obtain 2D and 3D brain EEG networks and respective alterations induced by 4-week LED-tPBM. All steps were performed using MATLAB except step six, which was performed using the eLORETA software. See text and Section A of the Supplementary Materials for details on each processing step. .

Steps 4 and 5 were performed to compute the gSVD across EEG measures in S1 and S8 for both groups. The concatenated matrix M_{gSVD} was used to identify the common Principal Components (PC) across four weeks and two groups using the native MATLAB function 'svd'. At the end of the analysis, we selected 12 gSVD-derived PCs with their respective weights, 1D time series, and corresponding topographies. Consequently, these extracted 12 gSVD components facilitated 2D topographies and 3D source localizations for the 12 EEG brain networks.

Step 6 was performed to quantify the source localization using eLORETA [36]. This enabled us to localize the 3D cortical sources of the 2D electric potential distribution of the 12 SVD components. This procedure produced 2D (sagittal, coronal, and axial) views for each brain EEG network.

Step 7 enabled the calculation of the normalized PSD of 12 SVD components for the respective time periods and in S1 of week 1 and S2 of week 4 for both groups using the MATLAB function "pwelch" (with a 20-sec window and 50% overlap).

Scheme 8. was required to compute the power changes in the EEG networks induced by the 4-week LED-tPBM. We obtained the spectrally averaged PSD power for each subject for each of the 5-f bands during TP1 and TP2 in sessions S1 and S8, followed by baseline normalization (nPSD) for all 12 SVD components, in both the tPBM and sham groups, and for TP1 and TP2. Furthermore, we computed differences in normalized network powers between S8 in week 4 and S1 in week 1 (i.e., $\Delta np = np\_S8 - np\_S1$) for each of the sham and tPBM groups in all 5-f bands during TP1 and TP2, respectively. Finally, significant differences of ΔnP between the tPBM versus sham groups were determined by performing two-sample, non-parametric tests [50,51] during TP1 and TP2 for each component in each frequency band at the significance level of $p < 0.05$ (marked by "*") and $p < 0.01$ (marked by "&"). A MATLAB function of "ranksum" was used as non-parametric permutation comparisons between the LED and sham groups in the 5 frequency bands and the 12 brain EEG networks.

3. Results

3.1. Repeated 4-week LED-tPBM significantly improves psychomotor vigilance

Group-averaged reaction times to PVT in both sham (n=11) and tPBM (n=11) groups during the 10-min stimulation over 4 weeks are plotted in Figure 4. Data were fitted using linear regression to observe the trend over time for both groups. Linear fitting showed a significant decrease in the reaction time for the tPBM group (p=0.002; red line), as shown in Figure 3. In contrast, the sham group did not achieve any significant improvement in reaction time over four weeks (p =0.07; blue line). This result demonstrates that repeated 10-min LED stimulation twice a week for four weeks improves psychomotor vigilance in healthy young participants. These results confirmed our first hypothesis.

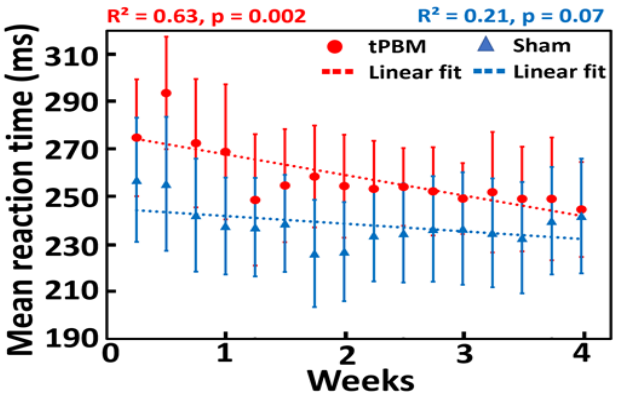

Preprints (www.preprints.org) | NOT PEER-REVIEWED | Posted: 12 July 2023 doi:10.20944/preprints202307.0795.v1

Figure 4. Effect of repeated 10-min LED-tPBM on the reaction time for the sham (n=11; blue) and tPBM (n=11; red) groups. Both dotted lines are linear fits to the sham (blue) and tPBM (red) groups with p-values of 0.002 and 0.07, respectively. Each data point reflects the mean reaction time averaged over each respective group during the 3-min PVT in each session from S1 to S8 over four weeks. Note that in each session (e.g., S1), two reaction times were recorded in TP1 and TP2, leading to a total of 16 data points over 4 weeks.

3.2. Justification of pooling EEG data during rest and PVT epochs in TP1 and TP2

In each experiment, we had a 10-min session (e.g., S1, S2, … S8), which consisted of two time periods (i.e., TP1 and TP2). Each TP included a 2-min rest and 3-min PVT epochs. Following the EEG data processing procedures, global $\overline{\boldsymbol{nPSD}}$ values were quantified for each 2-min rest and 3-min PVT epoch within each TP1 and TP2 in the sham and tPBM groups in each of the 5-*f* bands. Paired t-tests were performed on paired $\boldsymbol{nPSD(f)}$ values between the rest and PVT epochs in each respective 5-min period in S1 for each (sham and tPBM) group. We found no significant difference in $\overline{\boldsymbol{nPSD(f)}}$ between these two epochs within TP1 or TP2 across both groups and five frequency bands. Thus, we pooled the EEG data during the 2-min rest and 3-min PVT epochs together in each of TP1 and TP2 for further data analysis.

3.3. Acute effects and topographies of electrophysiology induced by initial LED-tPBM

To examine the acute effects of 10-min LED-tPBM, we first quantified and compared the global spectral values of $\overline{nPSD(f)}$ between the sham and tPBM groups during TP1 and TP2 in week 1, as shown in Figs. 5(a) and 5(b). These two figures clearly show a large difference in $\overline{nPSD}$ values between the two groups in the alpha frequency band (i.e., 8-13 Hz) during both TP1 and TP2 epochs. Next, the individual values of $\overline{nPSD(f)}$ from the 64 channels were used to generate topographical maps for each frequency band for both TP1 and TP2, as shown in Figure 5(c), using the EEGLAB extension in MATLAB. After careful statistical analysis, as described in Section 2.4.4, we observed significant enhancements in normalized EEG powers in (1) the medial parieto-occipital regions in the delta band and (2) the left frontal, left temporal, and medial occipital regions in the alpha band. These significant increases occurred only during the last 5 min of the 10-min tPBM (i.e., TP2) with a maximal increase of up to 30% with respect to those in the sham group in several cortical regions.

3.4. Longitudinal effects and topographies of electrophysiology induced by 4-week LED-tPBM

To investigate the longitudinal effects of the 4-week repeated LED-tPBM, the individual values of sham-subtracted $\overline{\boldsymbol{nPSD(f)}}$ (*ss*-$\overline{\boldsymbol{nPSD(f)}}$) from the 64 channels were first calculated and used to generate topographical maps in each frequency band for both TP1 and TP2 at week 4. Consequently, longitudinal effects were obtained by subtracting the *ss*-$\overline{\boldsymbol{nPSD(f)}}$ topographies in week 1 from those in week 4 for all 5-*f* bands during TP1 and TP2. The results are presented in Section B of the Supplementary Materials. The important lesson learned from this set of topographies was that the 4-week repeated LED-tPBM created widespread, significant increases in EEG spectral power across most scalp areas in all 5-*f* bands during TP2 with respect to those in the initial treatment. Accordingly, we implemented an advanced image-processing algorithm that would facilitate improved spatial resolution, as presented below.

Preprints (www.preprints.org) | NOT PEER-REVIEWED | Posted: 12 July 2023 doi:10.20944/preprints202307.0795.v1

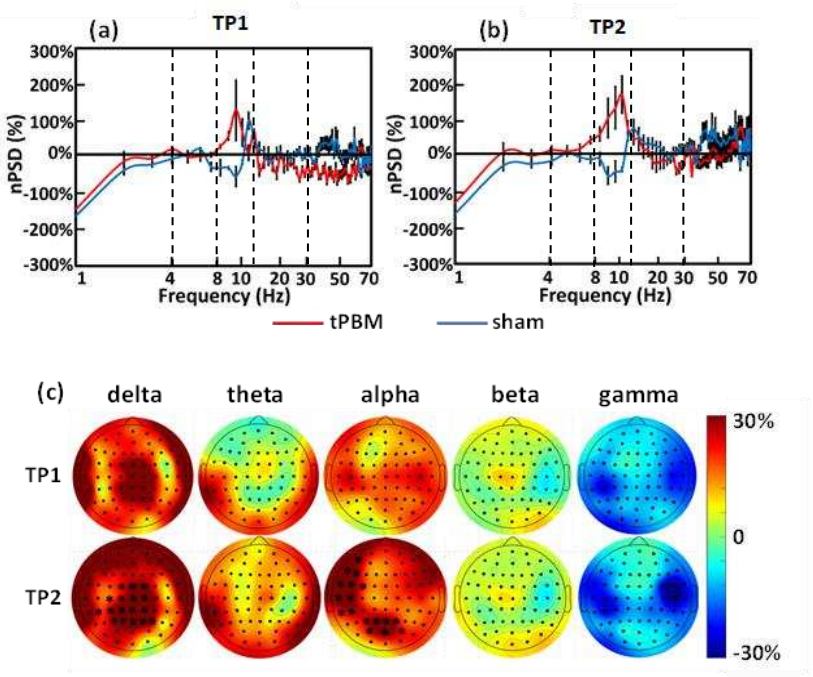

Figure 5. Normalized EEG power spectrum density (nPSD) plots averaged over all 64 channels from the sham (blue curve) and tPBM (red curve) groups during (a) TP1 and (b) TP2. Normalization was calculated with respect to the 2-min baseline taken at the beginning of the experiment without light stimulation (see Figure 1(d)). The x-axis denotes the EEG frequency in Hz, and the y-axis represents the percentage change in nPSD relative to the PSD during the 2-min baseline. (c) Topographic maps of the nPSD at 5-*f* bands. It shows statistical comparisons of channel-interpolated topographical alterations in nPSD between the sham (n=9) and tPBM (n=7) groups during TP1 and TP2 in week 1. The columns indicate the delta, theta, alpha, beta, and gamma bands. The color bar indicates the percentage change in nPSD with respect to the baseline. The "*" marks a p value < 0.05 for statistical significance after multivariate comparison correction.

3.5. Extraction and selection of gSVD components as EEG brain networks

Following Step 5 (Figure 3), we selected 12 gSVD-derived PCs with their respective weights, 1D time series, and corresponding topographies. These extracted 12 gSVD components facilitated 2D topographies and 3D source localizations for the 12 EEG brain networks. Specifically, Figure 6(a) shows the diagonal values of the 64 gSVD components with their respective rankings based on their weights in the EEG signal after gSVD. As shown in this figure, an exponential decay in weight was observed across all components. Any component whose weight decayed by more than 90% when compared to the first/most-weighted component was excluded from further analysis. Accordingly, 12 dominant components were selected using this criterion (marked in red in Figure 6(a)). These 12 components contributed 73% of the entire EEG signal (i.e., the area under the curve of the 12 components divided by that of all 64 components) and served as the 12 EEG brain networks.

Next, a power spectral analysis was conducted on the time course of each gSVD component using the native MATLAB function "pwelch". This resulted in a power spectral density (PSD) curve with a resolution of 0.125 Hz, ranging from 0 to 128 Hz for each gSVD component, subject, week, and TP (TP1 and TP2). Figure 6(b) illustrates an example of group-averaged PSD curves from the sham (blue curve) and tPBM (red curve) groups during TP2 for component two (i.e., gSVD #2) after appropriate filtering.

Preprints (www.preprints.org) | NOT PEER-REVIEWED | Posted: 12 July 2023 doi:10.20944/preprints202307.0795.v1

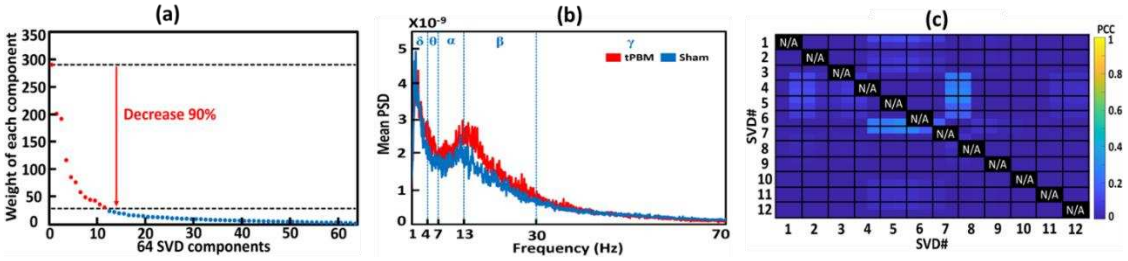

Figure 6. (a) Ranks and weights of all the 64 SVD components after gSVD. The x-axis indicates the ranks of the components, while the y-axis denotes the weight of each component. The weight-most 12 components are marked by red dots and selected for further data processing. The total weight of the 12 weight-most components (red) takes 70% of the total weight (all the dots). (b) Group-averaged PSD curves from the sham (blue) and tPBM (red) groups during TP2 for component two (SVD #2). Blue vertical lines mark the five EEG frequency bands, namely, delta (δ: 0.5-4 Hz), theta (θ: 4-7 Hz), alpha (α: 7-13 Hz), beta (β: 13-30 Hz), and gamma (γ: 30-70 Hz). (c) A correlation matrix to show group-averaged PCC values for every pair of the 12 networks. The vertical and horizontal axis depict the 12 gSVD components, and the color bar represents the PCC between each pair of the networks. Since all the self-correlations are meaningless, all the values along the diagonal line were marked as N/A (i.e., not applicable).

3.6. Construction of 3D EEG brain networks using eLORETA

After identifying the 12 components using gSVD, we considered them to represent or serve 12 EEG brain networks [36]. As these components were independent and orthogonal, they had minimal correlations. Pearson Correlation Coefficient (PCC) was performed between each pair of 20-minute (10 min for S1 and 10 min for S8) SVD components or networks for each subject to verify the least temporal correlations among all 12 gSVD components. Figure 6(c) depicts the group-averaged PCC values for every pair of the 12 networks. All the PCCs among these networks were less than 0.3, confirming orthogonal and independent activities among those networks.

Because each component has dimensions of 64 (for 64 electrodes in the spatial domain), it can form a 2D topography of the relative electrical potential (rEP) in the sensor space. Accordingly, the 12 extracted brain networks (i.e., the 12 gSVD components) are shown in Figure 7 (generated in step 5). To further compute the 3D models of the cortical/subcortical current density of each identified EEG brain network, eLORETA was utilized to facilitate axial, sagittal, and coronal views of the current density of neural activity, as shown in the middle three columns of Figure 7. The 3D rendered brain templates' top and side views of the left and right hemispheres are shown in the rightmost column of Figure 7. The yellow color on the rendered brain models indicates the binarized, associated cortical locations under a threshold of >75% of the maximum neural activity (i.e., cortical current density) in the network or 3D brain model. In other words, if the neural activity of the voxel lies within the top 25 percentile across all voxels in the brain model, the voxel was rendered yellow.

Using eLORETA, we identified key brain regions and cortical lobes with high neural activity (i.e., cortical electrical density) for each network, as listed in Table 2. For example, SVD #12 represents a network corresponding to the precentral gyrus and inferior parietal lobe, whereas SVD #1 and #3 reveal a network corresponding to the cingulate gyrus and precuneus.

Preprints (www.preprints.org) | NOT PEER-REVIEWED | Posted: 12 July 2023 doi:10.20944/preprints202307.0795.v1

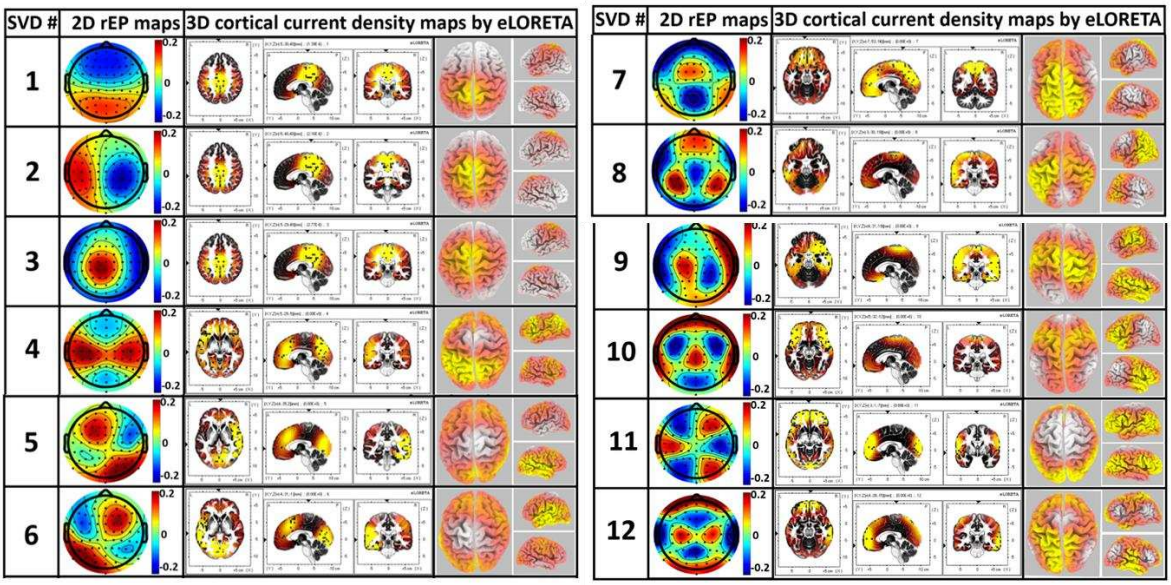

Figure 7. 2D rEP maps of 12 identified gSVD components with 3D source localization of cortical current density. For each of the two panels, the 2nd left most column shows the 2D rEP map, the middle three columns reveal the axial, sagittal, and coronial views for each rEP map, and the two right most columns depict the top and side views of the left and right hemisphere for 3D rendered brain templates. The yellow color in each brain model indicates the binarized cortical current density for a threshold of >75% of the maximum neuronal activity in respective brain models. The color bars show the rEP of the 'dipole' across the scalp (no unit).

Table 2. Main associated cortical lobes and regions for the 12 networks determined using eLORETA.

gSVD	Associated cerebral lobes	Associated brain regions
# 1	limbic lobe, parietal lobe	cingulate gyrus, precuneus
# 2	limbic lobe, parietal lobe	cingulate gyrus
# 3	limbic lobe, parietal lobe	cingulate gyrus, precuneus
# 4	Left: frontal, parietal lobe	Left: inferior frontal gyrus, inferior parietal lobule
# 5	Left: frontal, parietal, occipital lobe	Left: inferior frontal gyrus, inferior parietal lobule, precuneus
# 6	Right: frontal, parietal, occipital lobe	Right: inferior frontal gyrus, inferior parietal lobule, precuneus
# 7	medical frontal lobe, limbic lobe	medial frontal gyrus, anterior cingulate, cingulate gyrus
# 8	Frontal lobe, temporal lobe	Cingulate gyrus, lateral visual lobule
# 9	frontal lobe, parietal lobe	precentral gyrus, postcentral gyrus, inferior parietal lobule
# 10	Frontal lobe, limbic lobe	Cingulate gyrus
# 11	Right: occipital lobe	Right: middle occipital gyrus, cuneus
# 12	Frontal lobe, parietal lobe	Precentral gyrus, inferior parietal lobe

3.7. Alterations of EEG network powers induced by 4-week LED-tPBM

Following Step 8 (see Figure 3), we calculated the EEG power changes in the 12 gSVD-derived brain networks by 4-week tPBM in each of the five frequency bands from both groups in TP1 (Figure 8) and TP2 (Figure 9). Careful statistical analysis revealed that 4-week tPBM significantly enhanced brain EEG powers in several networks across all five frequency bands compared to sham stimulation. Moreover, such significant enhancements in network power occurred in more networks in TP2 than in TP1. Table 3 lists the number of EEG networks (i.e., the number of gSVD components) whose powers were significantly enhanced in TP1 and TP2 across the five frequency bands. The table clearly illustrates that networks #9 and #11 were consistently more stimulated in the theta, alpha, and beta bands throughout the 10-min tPBM in S8 than in S1. Similarly, networks #3, #5, and #6 were more power enhanced in the beta and gamma, theta and gamma, as well as theta and beta bands, respectively, throughout the tPBM period in S8 than in S1. Upon close inspection of the respective brain regions listed in Table 2, we concluded that 4-week LED-tPBM tended to increase the network

Preprints (www.preprints.org) | NOT PEER-REVIEWED | Posted: 12 July 2023 doi:10.20944/preprints202307.0795.v1

power in (1) the frontal, parietal lobe, and right occipital lobe in the theta, alpha, and beta bands; (2) the limbic and parietal lobes in the beta and gamma bands; and (3) the bilateral frontal, parietal, and occipital lobes in the theta, beta, and gamma bands.

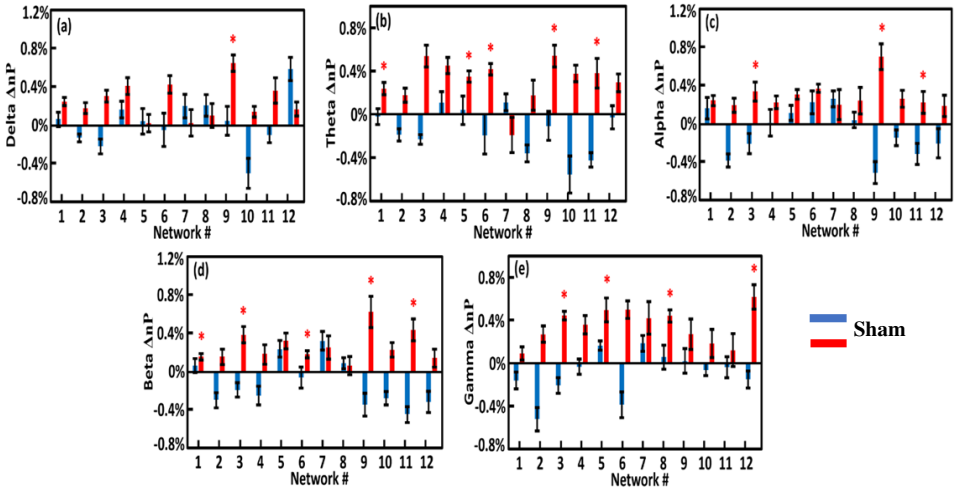

Figure 8. Group-level EEG power changes, Δnp, between S8 (in week 4) and S1 (in week 1) for 12 brain networks in (a) delta, (b) theta, (c) alpha, (d) beta, and (e) gamma bands during TP1 from the sham (blue) and tPBM (red) group. The standard error of the mean is represented by the error bars. The significant differences of Δnp between the two groups were determined using the two-sample non-parametric test at the significance level of $p<0.05$ and were indicated by '*'.

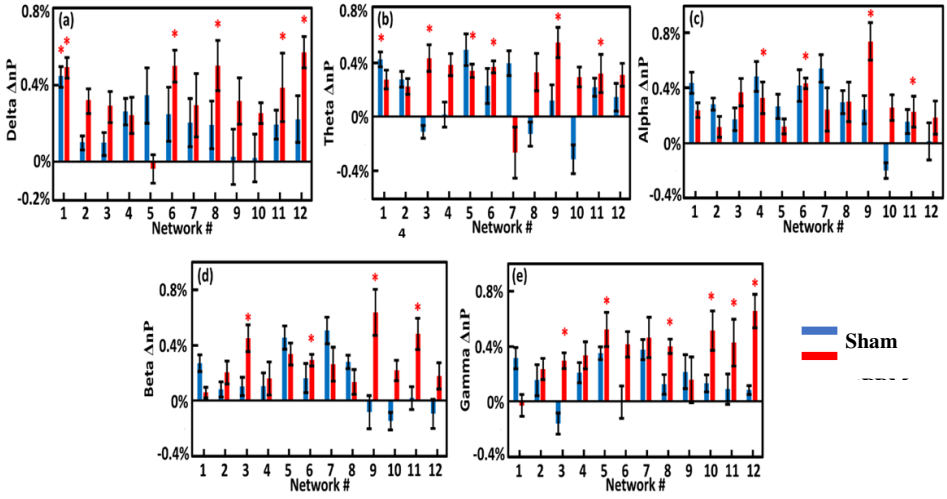

Figure 9. Group-level EEG power changes, Δnp, between S8 (in week 4) and S1 (in week 1) for 12 brain networks in (a) delta, (b) theta, (c) alpha, (d) beta, and (e) gamma bands during TP2 from the sham (blue) and tPBM (red) group. The standard error of the mean is represented by the error bars. The significant differences of Δnp between the two groups were determined using the two-sample non-parametric test at the significance level of $p<0.05$ and were indicated by '*'.

Preprints (www.preprints.org) | NOT PEER-REVIEWED | Posted: 12 July 2023 doi:10.20944/preprints202307.0795.v1

Table 3. EEG networks (i.e., gSVD components) that were stimulated by 4-week tPBM.

frequency band	TP1	TP2	Common networks in TP1 and TP2
delta	9	1 6 8 11 12	
theta	1 5 6 9 11	1 3 5 6 9 11	1 5 6 **9 11**
alpha	3 9 11	4 6 9 11	**9 11**
beta	1 3 6 9 11	3 6 9 11	3 6 **9 11**
gamma	3 5 8 12	3 5 8 10 11 12	3 5 8 12

Note: The network numbers written in red indicate new networks to appear only in TP2, not in TP1. TP1: time period 1; TP2: time period 2. **Bolded numbers** indicate the networks appeared three times.

4. Discussion

Because of its low cost, ease of use, non-invasiveness, and low irradiance, LED-based tPBM is a preferable choice for neuromodulation. In this study, we conducted 64-channel EEG measurements from 22 healthy human subjects while they performed the PVT task concurrently with right-forehead LED-tPBM at the beginning and end of a 4-week intervention protocol. Behavioral improvement in vigilance/attention (i.e., reaction time) was recorded each time during the treatment for four weeks. Our results showed a gradual and significant improvement in the reaction time in the tPBM-treated group over four weeks. Meanwhile, we found that LED-tPBM had significant effects on EEG network power in several brain networks in the respective frequency bands. To the best of our knowledge, this is the first study to demonstrate the effects of LED stimulation on the longitudinal improvement of psychomotor vigilance and the significant boost of electrophysiological functions in healthy subjects.

4.1. Effect of repeated 4-week LED-tPBM on gradual improvement of psychomotor vigilance

The longitudinal effects of repeated 4-week tPBM on reaction time are shown in Figure 3. These observations can be interpreted as follows. LED light delivery to the right forehead facilitates stimulation of metabolic activity in the electron transport chain of mitochondria, particularly in transmembrane protein complex IV (CCO) [31]. One of the major photoacceptors within the 600-900 nm range of red/NIR light is CCO [52]. This increase in CCO activity provides more neuronal metabolic energy (ATP) available for performing tasks. An increase in ATP levels increases cellular respiration, oxygenation, and hemodynamic activation [52]. Thus, with repeated tPBM over four weeks, LED stimulation improved attention by providing more energy in the form of ATP. This was reflected by the shortened reaction time in the tPBM-treated group. Furthermore, the reported observations demonstrate that significant improvement in psychomotor vigilance in healthy humans can be achieved by (1) repeated right-forehead tPBM over 4 weeks, (2) low irradiance of LED clusters if weekly routines of tPBM are carried out, and (3) a simple and sparse intervention schedule of 10-min per treatment and twice per week.

4.2. Acute EEG power enhancement of brain oscillations by LED-tPBM

In this study, we observed that LED-tPBM in S1 at week 1 enabled acute increases in EEG nPSD in the left frontal, left temporal, and medial occipital regions in the alpha band (Figure 5(c)). Cognitive stimulation and/or enhancement have been reported to be associated with an alpha power increase in the frontal and parietal regions [53–55]. Furthermore, the prefrontal cortex is known to play a key role in sustained attention, to be activated in response to tasks requiring vigilance/attention [56], and to control the executing function related to improving the reaction time during the task [57]. The salience network is also said to be present in the prefrontal cortex [58], responsible for the detection of distinct target inputs involved during PVT [58–60], and in charge of top-down short-term attention processing [61]. The ability of LED-tPBM to neuromodulate the electrophysiological activity of the

Preprints (www.preprints.org) | NOT PEER-REVIEWED | Posted: 12 July 2023 doi:10.20944/preprints202307.0795.v1

frontal cortex may account for the gradual and significant improvement in psychomotor vigilance in the tPBM-treated group.

An increased nPSD value in the parietal lobe was also observed under LED stimulation in the delta- and alpha-bands. (Figure 5(c)). The parietal lobe is said to modulate top-down attention, thus allowing faster reactions towards the stimulus [62–64]. Inferior parietal and frontal lobes are commonly observed during sustained attention [39]. Several studies have shown that the lateral frontal area and inferior parietal lobe together support executive control and attention maintenance [61,65,66]. In particular, the left inferior parietal lobe has been shown to be activated in subjects with a faster reaction time [62,63], and the parietal cortex is believed to be involved in spatial attention tasks, working memory, and decision-making [67,68]. Consequently, the increased EEG power in the inferior parietal lobe by LED-tPBM could explain the faster reaction time in the tPBM-treated subjects over time.

4.3. EEG power improvement globally in theta, beta, and gamma bands by Repeated LED-PBM

In this study, we observed that four weeks of LED-tPBM increased EEG nPSD globally in the theta, beta, and gamma bands (Figure S2 in Supplementary Materials). It has been reported that attention and efficient processing of the task are often associated with theta [69,70], beta [70], and gamma bands [71–74]. First, the theta band is often associated with efficient processing of cognitive tasks and attention [69,70,75]. It has been suggested that the prefrontal cortex exerts top-down control via inter-areal communication in the theta frequency range [61,76,77]. An increase in theta activity in the frontal areas indicates its involvement in working memory tasks [78–80]. Previous studies have revealed that an increase in theta and gamma power represents a neural correlation of working memory processing [81–83].

Second, beta oscillations are associated with cognitive functions, such as working memory [84–87], executive control of action [88–90], state of alert [70], and prevention of distraction [91,92]. Studies have suggested that beta oscillations convey moment-to-moment top-down modulatory signals to the lower sensory cortices, maintaining existing mental states [93,94]. Wrobel et. al. showed that beta band activity reflects arousal of the visual system during visual attention task [95]. Beta oscillatory responses have been considered to be related to motor and somatosensory functions [96]. The arousal of the visual system due to increased visual attention has also been thought to increase beta activity [95].

Finally, gamma oscillations have been extensively studied in cognitive processes engaged in attention, memory, and perception [83,97–101] and correlated with memory loading, formation, and maintenance [102–104]. Gamma oscillations have been proposed to play a role in the mechanisms of synaptic plasticity and memory formation [100,101,105] and have been shown to be modulated by cognitive processes engaged in spatial working memory in monkeys [85] and recognition memory tasks in humans [106]. Consequently, continuous and repeated intervention of LED-tPBM on the electrophysiological activities of the human brain over four weeks provided longitudinal modulations and increases in EEG power in key brain lobes, which can explain the gradual and significant improvement of psychomotor vigilance in the tPBM-treated group.

4.4. Large scale neural activities presented by gSVD-derived EEG brain networks

4.4.1. Similarity of gSVD-derived EEG brain networks to fMRI-defined networks

The application of gSVD with eLORETA enabled us to isolate and identify 12 intrinsic EEG brain networks, as shown in Figure 7, which accounted for 73% of the total contribution to the recorded EEG signal. This is consistent with the neural physiology that communication among neurons and functional activity in the human brain takes about 60-80% of the total energy [107]. We recognized spatial co-localizations between the gSVD-identified EEG networks and fMRI-recognized networks [108–113], by inspecting the active cortical localizations of each EEG network, as shown in Figure 7 and Table 2. Although EEG records electrophysiological oscillations at much higher frequencies with

Preprints (www.preprints.org) | NOT PEER-REVIEWED | Posted: 12 July 2023 doi:10.20944/preprints202307.0795.v1

a lower spatial resolution than fMRI, gSVD-derived EEG brain networks may reflect the same neural activity as fMRI-defined brain networks.

The first seven most weighted gSVD-derived EEG networks accounted for approximately 61% of the total EEG signal contribution. Networks #1, 2, 3, and 8 were found to be associated with the DMN, which is considered the most important and dominant network in the human brain **[114–116]**. Our results are consistent with this statement. Specifically, these networks associated with the DMN accounted for almost 43.6% and 60% of all EEG signals (64 components) and the 12 most weight/dominant brain networks. Thus, gSVD, along with eLORETA, offers a potentially feasible means of extracting the dominant DMN fluctuations of the human brain from EEG recordings. The left and right frontoparietal networks (L- and R-FPN) and executive control networks (ECN) were also identified using the gSVD algorithm and ranked as #4-7. These networks contributed to approximately 27.5% of the 12 dominant networks. The FPN is a network commonly observed during sustained attentional tasks [39]. The FPN is known to play an important role in cognition [113,117,118], attention, memory consolidation, and memory encoding [119–122]. Similarly, the ECN plays a crucial role in human executive control functions during sustained attentional tasks such as cognitive inhibition, inhibitory control, working memory, reasoning, memory, problem solving, and planning [119,123,124]. In short, the ability of the gSVD algorithm along with eLORETA to identify fMRI-defined, cognitive-sensitive networks (i.e., DMN, L-FPN, R-FPN, and ECN) based on measured EEG signals would expand the applications of EEG as a potential neural monitoring tool, along with a high temporal resolution.

4.4.2. Enhancement of network power by repeated LED-tPBM in selected brain networks

As listed in Table 3, the tPBM-treated group showed increased network power in several brain networks when compared with the sham group. First, networks #9 and #11 were consistently more stimulated in the theta, alpha, and beta bands after four weeks of repeated LED-tPBM. These two networks include the cortical regions of the precentral gyrus, postcentral gyrus, inferior parietal lobule, right middle occipital gyrus, and right cuneus. All brain regions are associated with cognitive function in humans. For example, the inferior frontal and parietal lobules play a major role in decision-making [125,126]; the parietal lobule is involved in information manipulation during working memory [127]; and the occipital lobe is required for perception [127]. Hence, we speculated that the LED-based tPBM induced the augmentation of vigilance as a result of the enhancement of network power in these cognition-related EEG cortical networks.

Meanwhile, networks #3, #5, and #6 were more power-enhanced in the respective frequency bands (see Table 3). These networks cover the brain regions of the cingulate gyrus, precuneus, right and left inferior frontal and parietal lobules, and precuneus. These regions are closely linked to human cognitive functions. In particular, the increase in beta power in parietal regions for faster reaction times has been related to attention processing in many fMRI studies [128–130]. In this study, enhancement of the parietal lobule could be related to the enhancement of the parietal attention network. It is also possible that beta band enhancement in frontoparietal regions reflects top-down attentional control [131]. These results are in agreement with a previous MEG study showing that beta oscillations serve as a mechanism for spreading attentional arousal among higher cortical areas [132]. Thus, the increase in beta band activity in all cortical areas could potentially explain the improvement in vigilance.

4.5. Limitation of the study and future work

This study has several limitations. First, the sample size was small; therefore, statistical power was limited. Second, the LEDs used in the study were two types of LED clusters at 660 nm and 810 nm, which prevented us from determining the exact contributions of the two light wavelengths to the significant effects of LED-tPBM. Third, the experimental design was unnecessarily complex and included two blocks of rest and a PVT task. Finally, EEG data were collected only during the tPBM intervention; no post-tPBM measurements were taken. Accordingly, further studies should include

a larger sample size to warrant excellent statistical power, using a single-wavelength (e.g., 810-nm LED) light source, with a simpler experimental design, and including post-tPBM assessments.

5. Conclusions

This sham-controlled study provided substantial evidence that supported or confirmed our three hypotheses: (1) repeated LED-tPBM of the right forehead of healthy subjects significantly improved psychomotor vigilance; (2) acute LED-tPBM significantly increased topographical EEG delta and alpha powers; (3) the four-week repeated LED-tPBM enhanced several brain network strengths (such as DMN, FPN, and ECN) in all five EEG frequency bands, compared to sham stimulation. Specifically, we showed, for the first time, acute increases in EEG delta and alpha powers during 10-min LED-tPBM while participants performed the PVT task. We also demonstrated that theta, beta, and gamma EEG powers significantly increased globally after four weeks of LED-tPBM. With a novel analysis of combining gSVD with eLORETA, we enabled to identify 12 independent and orthogonal brain networks in both sensor and brain space and found that these networks matched well with several fMRI-recognized networks. Our results clearly suggest that 4-week prefrontal LED-tPBM has the ability to neuromodulate the DMN, FPN, and ECN, which may indicate a possible causal effect between modulated brain networks and improved psychomotor vigilance outcomes. Future work should include more participants for stronger statistical power with a single-wavelength light source and a simpler experimental design.

Supplementary Materials: The following supporting information can be downloaded at: www.mdpi.com/xxx/s1.

Author Contributions: Conceptualization, X.W. and H.L.; methodology, A,C., X.W., and A.W.; software, A.C. and X.W.; validation, A.C, and X.W.; formal analysis, A.C. and X.W.. H.L.; resources, A.W. and H.L.; data curation, A.C. and X.W.; writing—original draft preparation, A.C. and X.W.; writing—review and editing, A.C. and X.W. and H.L.; visualization, A.C. and X.W.; supervision, H.L.; project administration, H.L.; funding acquisition, H.L. All authors have read and agreed to the published version of the manuscript. All authors have read and agreed to the published version of the manuscript.

Funding: This research was funded in part by NASA, Translational Research Institute for Space Health (TRISH).

Institutional Review Board Statement: The study was conducted according to the guidelines of the Declaration of Helsinki and approved by the Institutional Review Board of the University of Texas at Arlington (IRB protocol #2019-0333, approved on June 21, 2019).

Informed Consent Statement: Informed consent was obtained from all subjects involved in the study.

Data Availability Statement: The data presented in this study are available on request from the corresponding author.

Acknowledgments: The authors wish to express their sincere appreciation to Professor Jacek Dmochowski for his active collaboration and initial assistance with EEG data processing. The authors also would like to thank Drs. Tyrell Pruitt, Sadra Shahdadian, Nghi Truong, Hashini Wanniarachchi, and Ms. Shu Kang for their assistance with human data collection.

Conflicts of Interest: The authors declare no conflict of interest.

References

1. Wong-Riley, M.T.; Liang Hl Fau - Eells, J.T.; Eells Jt Fau - Chance, B.; Chance B Fau - Henry, M.M.; Henry Mm Fau - Buchmann, E.; Buchmann E Fau - Kane, M.; Kane M Fau - Whelan, H.T.; Whelan, H.T. Photobiomodulation directly benefits primary neurons functionally inactivated by toxins: role of cytochrome c oxidase. *The Journal of biological chemistry* **2005**, *280,6*, 4761-4771, doi:10.1074/jbc.M409650200.
2. Rojas, J.C.; Gonzalez-Lima, F. Low-level light therapy of the eye and brain. *Eye Brain* **2011**, *3*, 49-67, doi:10.2147/EB.S21391.
3. Huang, M.R.H.a.Y.Y. Mechanisms of photobiomodulaion in the brain. *Photobiomodulation in the Brain* **2019**.
4. Lampl, Y. Laser treatment for stroke. *Expert review of neurotherapeutics* **2007**, *7*, 961-965, doi:10.1586/14737175.7.8.961.

5. Naeser Ma Fau - Hamblin, M.R.; Hamblin, M.R. Potential for transcranial laser or LED therapy to treat stroke, traumatic brain injury, and neurodegenerative disease. *Photomedicine and laser surgery* **2011**, *29,7*, 443-446, doi:10.1089/pho.2011.9908.
6. Rojas, J.C.; Gonzalez-Lima, F. Neurological and psychological applications of transcranial lasers and LEDs. *Biochemical pharmacology* **2013**, *86,4*, 447-457, doi:10.1016/j.bcp.2013.06.012.
7. Eells, J.T.; Wong-Riley Mt Fau - VerHoeve, J.; VerHoeve J Fau - Henry, M.; Henry M Fau - Buchman, E.V.; Buchman Ev Fau - Kane, M.P.; Kane Mp Fau - Gould, L.J.; Gould Lj Fau - Das, R.; Das R Fau - Jett, M.; Jett M Fau - Hodgson, B.D.; Hodgson Bd Fau - Margolis, D.; et al. Mitochondrial signal transduction in accelerated wound and retinal healing by near-infrared light therapy. *Mitochondrion* **2004**, *vol. 4,5-6*, 559-567, doi:10.1016/j.mito.2004.07.033.
8. Rojas, J.C.; Lee J Fau - John, J.M.; John Jm Fau - Gonzalez-Lima, F.; Gonzalez-Lima, F. Neuroprotective effects of near-infrared light in an in vivo model of mitochondrial optic neuropathy. *The Journal of neuroscience : the official journal of the Society for Neuroscience* **2008**, *28,50*, 13511-13521, doi:10.1523/JNEUROSCI.3457-08.2008.
9. Gonzalez-Lima, F.; Barrett, D.W. Augmentation of cognitive brain functions with transcranial lasers. *Frontiers in systems neuroscience* **2014**, *8 36*, doi:10.3389/fnsys.2014.00036.
10. Gonzalez-Lima, F.; Auchter, A. Protection against neurodegeneration with low-dose methylene blue and near-infrared light. *Frontiers in cellular neuroscience* **2015**, *9*, 179, doi:10.3389/fncel.2015.00179.
11. Cassano, P.; Petrie, S.R.; Hamblin, M.R.; Henderson, T.A.; Iosifescu, D.V. Review of transcranial photobiomodulation for major depressive disorder: targeting brain metabolism, inflammation, oxidative stress, and neurogenesis. *Neurophotonics* **2016**, *3,3*, doi:10.1117/1.NPh.3.3.031404.
12. Mannu, P.; Maiello, M.; Spera, V.; Cassano, P. Transcranial Photobiomodulation for Down Syndrome. *Photobiomodulation, photomedicine, and laser surgery* **2019**, *37,10*, 579-580, doi:10.1089/photob.2019.4675.
13. Mannu, P.; Saccaro, L.F.; Spera, V.; Cassano, P. Transcranial Photobiomodulation to Augment Lithium in Bipolar-I Disorder. *Photobiomodulation, photomedicine, and laser surgery* **2019**, *37,10*, 57-578, doi:10.1089/photob.2019.4674.
14. Caldieraro, M.A.; Cassano, P. Transcranial and systemic photobiomodulation for major depressive disorder: A systematic review of efficacy, tolerability and biological mechanisms. *Journal of affective disorders* **2019**, *243*, 262-273, doi:10.1016/j.jad.2018.09.048.
15. Hipskind, S.G.; Grover, F.L., Jr.; Fort, T.R.; Helffenstein, D.; Burke, T.J.; Quint, S.A.; Bussiere, G.; Stone, M.; Hurtado, T. Pulsed Transcranial Red/Near-Infrared Light Therapy Using Light-Emitting Diodes Improves Cerebral Blood Flow and Cognitive Function in Veterans with Chronic Traumatic Brain Injury: A Case Series. *Photomedicine and laser surgery* **2021**, doi:10.1089/pho.2018.4489.
16. Figueiro Longo, M.G.; Tan, C.O.; Chan, S.T.; Welt, J.; Avesta, A.; Ratai, E.; Mercaldo, N.D.; Yendiki, A.; Namati, J.; Chico-Calero, I.; et al. Effect of Transcranial Low-Level Light Therapy vs Sham Therapy Among Patients With Moderate Traumatic Brain Injury: A Randomized Clinical Trial. *JAMA network open* **2020**, *3,9 e2017337*, doi:10.1001/jamanetworkopen.2020.17337.
17. Berman, M.H.; Halper, J.P.; Nichols, T.W.; Jarrett, H.; Lundy, A.; Huang, J.H. Photobiomodulation with Near Infrared Light Helmet in a Pilot, Placebo Controlled Clinical Trial in Dementia Patients Testing Memory and Cognition. *Journal of neurology and neuroscience* **2017**, *8,1*, 176, doi:10.21767/2171-6625.1000176.
18. Nizamutdinov, D.; Qi, X.; Berman, M.H.; Dougal, G.; Dayawansa, S.; Wu, E.; Yi, S.S.; Stevens, A.B.; Huang, J.H. Transcranial Near Infrared Light Stimulations Improve Cognition in Patients with Dementia. *Aging and disease* **2021**, *12,4*, 954-963, doi:10.14336/AD.2021.0229.
19. Dougal, G.A.-O.; Ennaceur, A.A.-O.; Chazot, P.L. Effect of Transcranial Near-Infrared Light 1068 nm Upon Memory Performance in Aging Healthy Individuals: A Pilot Study. *Photobiomodulation, photomedicine, and laser surgery* **2021**, *39,10*, 654-660, doi:10.1089/photob.2020.4956.
20. Chan, A.A.-O.X.; Lee, T.A.-O.; Yeung, M.A.-O.; Hamblin, M.A.-O. Photobiomodulation improves the frontal cognitive function of older adults. *International journal of geriatric psychiatry* **2019**, *34,2*, 369-377, doi:10.1002/gps.5039.
21. Chan, A.S.; Lee, T.L.; Hamblin, M.R.; Cheung, M.C. Photobiomodulation Enhances Memory Processing in Older Adults with Mild Cognitive Impairment: A Functional Near-Infrared Spectroscopy Study. *Journal of Alzheimer's disease* **2021**, *83,4*, 1471-1480, doi:10.3233/JAD-201600.
22. Chan AS, L.T., Sze S, et al. Photobiomodulation Improves Memory in Mild Cognitive Impairment: Three Case Reports. *Alzheimers Dis Dement* **2021**, *5(1)*, 126-131.
23. Hamblin, M.R.; Salehpour, F. Photobiomodulation of the Brain: Shining Light on Alzheimer's and Other Neuropathological Diseases. *Journal of Alzheimer's disease* **2019**, *83,4*, 1395-1397, doi:10.3233/JAD-210743.
24. Salehpour, F.; Khademi, M.; Hamblin, M.R. Photobiomodulation Therapy for Dementia: A Systematic Review of Pre-Clinical and Clinical Studies. *Journal of Alzheimer's disease* **2021**, *83,4*, 1431-1452, doi:10.3233/JAD-210029.
25. Enengl, J.; Hamblin, M.R.; Dungel, P. Photobiomodulation for Alzheimer's Disease: Translating Basic Research to Clinical Application. *Journal of Alzheimer's disease* **2020**, *75,4*, 1073-1082, doi:10.3233/JAD-191210.

26. X. Wang, J.D., M. Husain, F. Gonzalez-Lima, and H. Liu. Proceedings# 18. Transcranial infrared brain stimulation modulates EEG alpha power. *BRain Stimulation: Basic, Translational, and Clinical Research in Neuromodulation* **2017**, *10*, e67-e69.
27. Wang, X.; Tian, F.; Soni, S.S.; Gonzalez-Lima, F.; Liu, H. Interplay between up-regulation of cytochrome-c-oxidase and hemoglobin oxygenation induced by near-infrared laser. *Scientific reports* **2016**, *6*, doi:10.1038/srep30540.
28. Wu Q Fau - Wang, X.; Wang X Fau - Liu, H.; Liu H Fau - Zeng, L.; Zeng, L. Learning Hemodynamic Effect of Transcranial Infrared Laser Stimulation Using Longitudinal Data Analysis. *." IEEE journal of biomedical and health informatics* **2020**, *24,6*, 1772-1779, doi:10.1109/JBHI.2019.2951772.
29. Pruitt, T.; Wang, X.; Wu, A.; Kallioniemi, E.; Husain, M.M.; Liu, H.A.-O. Transcranial Photobiomodulation (tPBM) With 1,064-nm Laser to Improve Cerebral Metabolism of the Human Brain In Vivo. *Lasers in surgery and medicine* **2020**, *52,9*, 807-813, doi:10.1002/lsm.23232.
30. Saucedo, C.L.; Courtois, E.C.; Wade, Z.S.; Kelley, M.N.; Kheradbin, N.; Barrett, D.W.; Gonzalez-Lima, F. Transcranial laser stimulation: Mitochondrial and cerebrovascular effects in younger and older healthy adults. *Brain stimulation* **2021**, *14,2*, 440-449, doi:10.1016/j.brs.2021.02.011.
31. Zomorrodi, R.; Loheswaran, G.; Pushparaj, A.; Lim, L. Pulsed Near Infrared Transcranial and Intranasal Photobiomodulation Significantly Modulates Neural Oscillations: a pilot exploratory study. *Scientific reports* **2019**, *9*, doi:10.1038/s41598-019-42693-x.
32. Vargas, E.; Barrett, D.W.; Saucedo, C.L.; Huang, L.D.; Abraham, J.A.; Tanaka, H.; Haley, A.P.; Gonzalez-Lima, F. Beneficial neurocognitive effects of transcranial laser in older adults. *Lasers in medical science* **2017**, *32,5*, 1153-1162, doi:10.1007/s10103-017-2221-y.
33. Ghaderi, A.H.; Jahan, A.; Akrami, F.; Moghadam Salimi, M.A.-O. Transcranial photobiomodulation changes topology, synchronizability, and complexity of resting state brain networks. *Journal of neural engineering* **2021**, *18,4*, doi:10.1088/1741-2552/abf97c.
34. Spera, V.; Sitnikova, T.; Ward, M.J.; Farzam, P.; Hughes, J.; Gazecki, S.; Bui, E.; Maiello, M.; De Taboada, L.; Hamblin, M.R.; et al. Pilot Study on Dose-Dependent Effects of Transcranial Photobiomodulation on Brain Electrical Oscillations: A Potential Therapeutic Target in Alzheimer's Disease. *Journal of Alzheimer's disease* **2021**, *83,4*, 1481-1498, doi:10.3233/JAD-210058.
35. Wang, X.; Dmochowski, J.P.; Zeng, L.; Kallioniemi, E.; Husain, M.; Gonzalez-Lima, F.; Liu, H.A.-O. Transcranial photobiomodulation with 1064-nm laser modulates brain electroencephalogram rhythms. *Neurophotonics* **2019**, *6,2*, doi:10.1117/1.NPh.6.2.025013.
36. Wang, X.; Wanniarachchi, H.; Wu, A.; Liu, H. Combination of Group Singular Value Decomposition and eLORETA Identifies Human EEG Networks and Responses to Transcranial Photobiomodulation. *Frontiers in human neuroscience* **2022**, *16*, doi:10.3389/fnhum.2022.853909.
37. Barrett, D.W.; Gonzalez-Lima, F. Transcranial infrared laser stimulation produces beneficial cognitive and emotional effects in humans. *Neuroscience* **2013**, *230*, 13-23, doi:10.1016/j.neuroscience.2012.11.016.
38. Blanco, N.J.; Maddox, W.T.; Gonzalez-Lima, F. Improving executive function using transcranial infrared laser stimulation. *Journal of neuropsychology* **2017**, *11,1*, 14-25, doi:10.1111/jnp.12074.
39. Drummond, S.P.; Bischoff-Grethe A Fau - Dinges, D.F.; Dinges Df Fau - Ayalon, L.; Ayalon L Fau - Mednick, S.C.; Mednick Sc Fau - Meloy, M.J.; Meloy, M.J. The neural basis of the psychomotor vigilance task. *Sleep* **2005**, *28,9*, 1059-1068.
40. Hwang, J.; Castelli, D.M.; Gonzalez-Lima, F. Cognitive enhancement by transcranial laser stimulation and acute aerobic exercise. *Lasers in medical science* **2016**, *31,6*, 1151-1160, doi:10.1007/s10103-016-1962-3.
41. Wang, X.; Wanniarachchi, H.; Wu, A.; Gonzalez-Lima, F.; Liu, H. Transcranial photobiomodulation and thermal stimulation induce distinct topographies of EEG alpha and beta power changes in healthy humans. *Scientific reports* **2021**, *11,1*, doi:10.1038/s41598-021-97987-w.
42. Van Dongen, H.P.; Maislin G Fau - Mullington, J.M.; Mullington Jm Fau - Dinges, D.F.; Dinges, D.F. The cumulative cost of additional wakefulness: dose-response effects on neurobehavioral functions and sleep physiology from chronic sleep restriction and total sleep deprivation. *Sleep* **2003**, *26,2*, 117-126, doi:10.1093/sleep/26.2.117.
43. informatics., P. PVT workfit. Available online: https://pulsarinformatics.com/products/pvtworkfit (accessed on
44. Delorme, A.; Makeig, S. EEGLAB: an open source toolbox for analysis of single-trial EEG dynamics including independent component analysis. *Journal of neuroscience methods* **2004**, *134,1*, 9-21, doi:10.1016/j.jneumeth.2003.10.009.
45. Asadi, N.A.-O.; Wang, Y.; Olson, I.; Obradovic, Z. A heuristic information cluster search approach for precise functional brain mapping. *Human brain mapping* **2020**, *41, 9*, 2263-2280, doi:10.1002/hbm.24944.
46. Hyvärinen, A.; Oja, E. Simple neuron models for independent component analysis. *International journal of neural systems* **996**, *7,6*, 671-687, doi:10.1142/s0129065796000646.
47. The R Project for Statistical Computing. Available online: https://www.r-project.org/ (accessed on

48. Popov, T.; Oostenveld, R.; Schoffelen, J.M. FieldTrip Made Easy: An Analysis Protocol for Group Analysis of the Auditory Steady State Brain Response in Time, Frequency, and Space. *Frontiers in neuroscience* **2018**, *12*, 711, doi:10.3389/fnins.2018.00711.
49. Oostenveld, R.; Fries P Fau - Maris, E.; Maris E Fau - Schoffelen, J.-M.; Schoffelen, J.M. FieldTrip: Open source software for advanced analysis of MEG, EEG, and invasive electrophysiological data. *Computational intelligence and neuroscience* **2011**, *2011*, doi:10.1155/2011/156869.
50. Clements, G.M.; Bowie, D.C.; Gyurkovics, M.; Low, K.A.; Fabiani, M.; Gratton, G. Spontaneous Alpha and Theta Oscillations Are Related to Complementary Aspects of Cognitive Control in Younger and Older Adults. *Frontiers in human neuroscience* **2021**, *15 621620*, doi:10.3389/fnhum.2021.621620.
51. MathWorks. Permutation Test. Available online: https://www.mathworks.com/matlabcentral/fileexchange/63276-permutation-test (accessed on
52. Jahan, A.; Nazari, M.A.; Mahmoudi, J.; Salehpour, F.; Salimi, M.A.-O. Transcranial near-infrared photobiomodulation could modulate brain electrophysiological features and attentional performance in healthy young adults. *Lasers in medical science* **2019**, *34,6*, 1193-1200, doi:10.1007/s10103-018-02710-3.
53. Başar, E. A review of gamma oscillations in healthy subjects and in cognitive impairment. *International journal of psychophysiology : official journal of the International Organization of Psychophysiology* **2013**, *90,2*, 99-117, doi:10.1016/j.ijpsycho.2013.07.005.
54. Tanaka, M.; Shigihara Y Fau - Ishii, A.; Ishii A Fau - Funakura, M.; Funakura M Fau - Kanai, E.; Kanai E Fau - Watanabe, Y.; Watanabe, Y. Effect of mental fatigue on the central nervous system: an electroencephalography study. *Behavioral and brain functions : BBF* **2012**, *8 48*, doi:10.1186/1744-9081-8-48.
55. Palva, S.; Palva, J.M. Functional roles of alpha-band phase synchronization in local and large-scale cortical networks. *Frontiers in psychology* **2011**, *2*, 204, doi:10.3389/fpsyg.2011.00204.
56. Naeser, M.A.; Saltmarche A Fau - Krengel, M.H.; Krengel Mh Fau - Hamblin, M.R.; Hamblin Mr Fau - Knight, J.A.; Knight, J.A. Improved cognitive function after transcranial, light-emitting diode treatments in chronic, traumatic brain injury: two case reports. *Photomedicine and laser surgery* **2011**, *29,5*, 351-358, doi:10.1089/pho.2010.2814.
57. Tekin, S.; Cummings, J.L. Frontal-subcortical neuronal circuits and clinical neuropsychiatry: an update. *Journal of psychosomatic research* **2002**, *53,2*, 647-654, doi:10.1016/s0022-3999(02)00428-2.
58. Power, J.D.; Cohen Al Fau - Nelson, S.M.; Nelson Sm Fau - Wig, G.S.; Wig Gs Fau - Barnes, K.A.; Barnes Ka Fau - Church, J.A.; Church Ja Fau - Vogel, A.C.; Vogel Ac Fau - Laumann, T.O.; Laumann To Fau - Miezin, F.M.; Miezin Fm Fau - Schlaggar, B.L.; Schlaggar Bl Fau - Petersen, S.E.; et al. Functional network organization of the human brain. *Neuron* **2011**, *72,4*, 665-678, doi:10.1016/j.neuron.2011.09.006.
59. Kucyi, A.; Hodaie M Fau - Davis, K.D.; Davis, K.D. Lateralization in intrinsic functional connectivity of the temporoparietal junction with salience- and attention-related brain networks. *Journal of neurophysiology* **2012**, *108,12*, 3382-3392, doi:10.1152/jn.00674.2012.
60. Menon, V.; Uddin, L.Q. Saliency, switching, attention and control: a network model of insula function. *Brain structure & function* **2010**, *214,5-6*, 655-667, doi:10.1007/s00429-010-0262-0.
61. Hopfinger, J.B.; Buonocore Mh Fau - Mangun, G.R.; Mangun, G.R. The neural mechanisms of top-down attentional control. *Nature neuroscience* **2000**, *3,3*, 284-291, doi:10.1038/72999.
62. Culham, J.C.; Cavanagh P Fau - Kanwisher, N.G.; Kanwisher, N.G. Attention response functions: characterizing brain areas using fMRI activation during parametric variations of attentional load. *Neuron* **2001**, *32,4*, 737-745, doi:10.1016/s0896-6273(01)00499-8.
63. Sturm, W.; Willmes, K. On the functional neuroanatomy of intrinsic and phasic alertness. *NeuroImage* **2001**, *14,1*, doi:10.1006/nimg.2001.0839.
64. Yamasaki, H.; LaBar Ks Fau - McCarthy, G.; McCarthy, G. Dissociable prefrontal brain systems for attention and emotion. *Proceedings of the National Academy of Sciences of the United States of America* **2002**, *99,17*, 11447-11451, doi:10.1073/pnas.182176499.
65. DiFrancesco, M.A.-O.; Van Dyk, T.; Altaye, M.; Drummond, S.P.A.; Beebe, D.W. Network-based Responses to the Psychomotor Vigilance Task during Lapses in Adolescents after Short and Extended Sleep. *Scientific reports* **2019**, *9,1 13913*, doi:10.1038/s41598-019-50180-6.
66. Langner, R.; Eickhoff, S.B. Sustaining attention to simple tasks: a meta-analytic review of the neural mechanisms of vigilant attention. *Psychological bulletin* **2013**, *139,4*, 870-900, doi:10.1037/a0030694.
67. Parvizi, J.; Wagner, A.D. Memory, Numbers, and Action Decision in Human Posterior Parietal Cortex. *Neuron* **2018**, *97,1*, 7-10, doi:10.1016/j.neuron.2017.12.031.
68. Qi, J.; Li, B.Z.; Zhang, Y.; Pan, B.; Gao, Y.H.; Zhan, H.; Liu, Y.; Shao, Y.C.; Zhang, X. Altered insula-prefrontal functional connectivity correlates to decreased vigilant attention after total sleep deprivation. *Sleep medicine* **2021**, *84*, 187-194, doi:10.1016/j.sleep.2021.05.037.
69. Aftanas, L.I.; Golocheikine, S.A. Human anterior and frontal midline theta and lower alpha reflect emotionally positive state and internalized attention: high-resolution EEG investigation of meditation. *Neuroscience letters* **2001**, *310, 1*, 57-60, doi:0.1016/s0304-3940(01)02094-8.
70. R. Stern, R., W., & Quigley, K. Psychophysiological Recording. **2022**.

71. Zheng, C.; Bieri, K.W.; Hsiao, Y.T.; Colgin, L.L. Spatial Sequence Coding Differs during Slow and Fast Gamma Rhythms in the Hippocampus. *Neuron* **2016**, *89,2*, 398-408, doi:10.1016/j.neuron.2015.12.005.
72. Colgin, L.L. Do slow and fast gamma rhythms correspond to distinct functional states in the hippocampal network? *Brain research* **2015**, *1621*, doi:10.1016/j.brainres.2015.01.005.
73. Colgin, L.L. Theta-gamma coupling in the entorhinal-hippocampal system. *Current opinion in neurobiology* **2015**, *31*, 45-50, doi:10.1016/j.conb.2014.08.001.
74. Colgin, L.L. Rhythms of the hippocampal network. *Nature reviews. Neuroscience* **2016**, *17,4*, 239-249, doi:10.1038/nrn.2016.21.
75. Klimesch, W. EEG alpha and theta oscillations reflect cognitive and memory performance: a review and analysis. *Brain research. Brain research reviews* **1999**, *29,2-3*, 169-195, doi:10.1016/s0165-0173(98)00056-3.
76. Botvinick, M.M. Conflict monitoring and decision making: reconciling two perspectives on anterior cingulate function. *Cognitive, affective & behavioral neuroscience* **2007**, *7,4*, 355 - 366, doi:10.3758/cabn.7.4.356.
77. Helfrich, R.F.; Knight, R.T. Oscillatory Dynamics of Prefrontal Cognitive Control. *Trends in cognitive sciences* **2016**, *20, 12*, 916-930, doi:10.1016/j.tics.2016.09.007.
78. Fernández, A.; Pinal, D.; Díaz, F.; Zurrón, M. Working memory load modulates oscillatory activity and the distribution of fast frequencies across frontal theta phase during working memory maintenance. *Neurobiology of learning and memory* **2021**, *183*, doi:10.1016/j.nlm.2021.107476.
79. DeCoteau, W.E.; Thorn C Fau - Gibson, D.J.; Gibson Dj Fau - Courtemanche, R.; Courtemanche R Fau - Mitra, P.; Mitra P Fau - Kubota, Y.; Kubota Y Fau - Graybiel, A.M.; Graybiel, A.M. Oscillations of local field potentials in the rat dorsal striatum during spontaneous and instructed behaviors. *Journal of neurophysiology* **2007**, *97,5*, 3800-3805, doi:10.1152/jn.00108.2007.
80. Liebe, S.; Hoerzer Gm Fau - Logothetis, N.K.; Logothetis Nk Fau - Rainer, G.; Rainer, G. Theta coupling between V4 and prefrontal cortex predicts visual short-term memory performance. *Nature neuroscience* **2012**, *15,3* 456-462, doi:10.1038/nn.3038.
81. Sauseng, P.; Klimesch, W. What does phase information of oscillatory brain activity tell us about cognitive processes? **2008**.
82. Hsieh, L.T.; Ranganath, C. Frontal midline theta oscillations during working memory maintenance and episodic encoding and retrieval. *NeuroImage* **2014**, *85 Pt 2*, doi:10.1016/j.neuroimage.2013.08.003.
83. Singer, W. Synchronization of cortical activity and its putative role in information processing and learning. *Annual review of physiology* **1993**, *55*, 349-374, doi:10.1146/annurev.ph.55.030193.002025.
84. Lundqvist, M.; Herman P Fau - Lansner, A.; Lansner, A. Theta and gamma power increases and alpha/beta power decreases with memory load in an attractor network model. *Journal of cognitive neuroscience* **2011**, *23,10* 3008-3020, doi:10.1162/jocn_a_00029.
85. Lundqvist, M.; Rose, J.; Herman, P.; Brincat, S.L.; Buschman, T.J.; Miller, E.K. Gamma and Beta Bursts Underlie Working Memory. *Neuron* **2016**, *90,1*, 152-164, doi:10.1016/j.neuron.2016.02.028.
86. Lundqvist, M.; Herman, P.; Warden, M.A.-O.; Brincat, S.L.; Miller, E.K. Gamma and beta bursts during working memory readout suggest roles in its volitional control. *Nature communications* **2018**, *9,1*, 394, doi:10.1038/s41467-017-02791-8.
87. Miller, E.K.; Lundqvist, M.; Bastos, A.M. Working Memory 2.0. *Neuron* **2018**, *100,2*, 463-475, doi:10.1016/j.neuron.2018.09.023.
88. Swann, N.; Tandon N Fau - Canolty, R.; Canolty R Fau - Ellmore, T.M.; Ellmore Tm Fau - McEvoy, L.K.; McEvoy Lk Fau - Dreyer, S.; Dreyer S Fau - DiSano, M.; DiSano M Fau - Aron, A.R.; Aron, A.R. Intracranial EEG reveals a time- and frequency-specific role for the right inferior frontal gyrus and primary motor cortex in stopping initiated responses. *The Journal of neuroscience : the official journal of the Society for Neuroscience* **2009**, *29,40*, 12675-12685, doi:10.1523/JNEUROSCI.3359-09.2009.
89. Ruiz, M.H.; Strübing F Fau - Jabusch, H.-C.; Jabusch Hc Fau - Altenmüller, E.; Altenmüller, E. EEG oscillatory patterns are associated with error prediction during music performance and are altered in musician's dystonia. *NeuroImage* **2011**, *55,4*, 1791-1803, doi:10.1016/j.neuroimage.2010.12.050.
90. Wessel, J.R.; Conner Cr Fau - Aron, A.R.; Aron Ar Fau - Tandon, N.; Tandon, N. Chronometric electrical stimulation of right inferior frontal cortex increases motor braking. *The Journal of neuroscience : the official journal of the Society for Neuroscience* **2013**, *33,50*, 19611-19619, doi:10.1523/JNEUROSCI.3468-13.2013.
91. Hanslmayr, S.; Matuschek, J.; Fellner, M.C. Entrainment of prefrontal beta oscillations induces an endogenous echo and impairs memory formation. **2014**.
92. Zavala, B.A.; Jang, A.I.; Zaghloul, K.A.-O. Human subthalamic nucleus activity during non-motor decision making. *eLife* **2017**, *6*, doi:10.7554/eLife.31007.
93. Engel, A.K.; Fries, P. Beta-band oscillations--signalling the status quo? *Current opinion in neurobiology* **2010**, *20,2*, 156-165, doi:10.1016/j.conb.2010.02.015.
94. Bressler, S.L., and Craig G Richter. Interareal oscillatory synchronization in top-down neocortical processing. *Current opinion in neurobiology* **2015**, *31*, 62-66, doi:10.1016/j.conb.2014.08.010.
95. Wróbel, A. Beta activity: a carrier for visual attention. *Acta neurobiologiae experimentalis* **2000**, *60,2*, 247-260.

96. Pfurtscheller, G.; Stancák A Jr Fau - Neuper, C.; Neuper, C. Post-movement beta synchronization. A correlate of an idling motor area? *Electroencephalography and clinical neurophysiology* **1996**, *98,4* 281-293, doi:10.1016/0013-4694(95)00258-8.
97. Hughes, J.R. RESPONSES FROM THE VISUAL CORTEX OF UNANESTHETIZED MONKEYS. **1964**.
98. Tallon-Baudry, C.; Bertrand, O. Oscillatory gamma activity in humans and its role in object representation. *Trends in cognitive sciences* **1999**, *3,4*, 151-162, doi:10.1016/s1364-6613(99)01299-1.
99. Jensen, O.; Kaiser J Fau - Lachaux, J.-P.; Lachaux, J.P. Human gamma-frequency oscillations associated with attention and memory. *Trends in neurosciences* **2007**, *30,7*, 317-324, doi:10.1016/j.tins.2007.05.001.
100. Fries, P. Neuronal gamma-band synchronization as a fundamental process in cortical computation. *Annual review of neuroscience* **2009**, *32*, 209-224, doi:10.1146/annurev.neuro.051508.135603.
101. Düzel, E.; Penny Wd Fau - Burgess, N.; Burgess, N. Brain oscillations and memory. *Current opinion in neurobiology* **2010**, *20,2*, 143-149, doi:10.1016/j.conb.2010.01.004.
102. Howard, M.W.; Rizzuto Ds Fau - Caplan, J.B.; Caplan Jb Fau - Madsen, J.R.; Madsen Jr Fau - Lisman, J.; Lisman J Fau - Aschenbrenner-Scheibe, R.; Aschenbrenner-Scheibe R Fau - Schulze-Bonhage, A.; Schulze-Bonhage A Fau - Kahana, M.J.; Kahana, M.J. Gamma oscillations correlate with working memory load in humans. *Cerebral cortex (New York, N.Y. : 1991)* **2003**, *13,12*, 1369-1374, doi:10.1093/cercor/bhg084.
103. Sederberg, P.B.; Schulze-Bonhage A Fau - Madsen, J.R.; Madsen Jr Fau - Bromfield, E.B.; Bromfield Eb Fau - McCarthy, D.C.; McCarthy Dc Fau - Brandt, A.; Brandt A Fau - Tully, M.S.; Tully Ms Fau - Kahana, M.J.; Kahana, M.J. Hippocampal and neocortical gamma oscillations predict memory formation in humans. *Cerebral cortex (New York, N.Y. : 1991)* **2007**, *17,5*, 1190-1196, doi:10.1093/cercor/bhl030.
104. Roux, F.; Wibral M Fau - Mohr, H.M.; Mohr Hm Fau - Singer, W.; Singer W Fau - Uhlhaas, P.J.; Uhlhaas, P.J. Gamma-band activity in human prefrontal cortex codes for the number of relevant items maintained in working memory. *The Journal of neuroscience : the official journal of the Society for Neuroscience* **2012**, *32,36*, 12411-12420, doi:10.1523/JNEUROSCI.0421-12.2012.
105. Buzsáki, G.; Wang, X.J. Mechanisms of gamma oscillations. *Annual review of neuroscience* **2012**, *35*, 203-225, doi:10.1146/annurev-neuro-062111-150444.
106. Kucewicz, M.T.; Cimbalnik, J.; Matsumoto, J.Y.; Brinkmann, B.H.; Bower, M.R.; Vasoli, V.; Sulc, V.; Meyer, F.; Marsh, W.R.; Stead, S.M.; et al. High frequency oscillations are associated with cognitive processing in human recognition memory. *Brain : a journal of neurology* **2014**, *137*, 2231-2244, doi:10.1093/brain/awu149.
107. Raichle, M.E.; Snyder, A.Z. A default mode of brain function: a brief history of an evolving idea. *NeuroImage* **2007**, *37,4*, 1083-1090, doi:10.1016/j.neuroimage.2007.02.041.
108. Aoki, Y.; Ishii, R.; Pascual-Marqui, R.D.; Canuet, L.; Ikeda, S.; Hata, M.; Imajo, K.; Matsuzaki, H.; Musha, T.; Asada, T.; et al. Detection of EEG-resting state independent networks by eLORETA-ICA method. *Frontiers in human neuroscience* **10 Feb. 2015**, *9 31*, doi:10.3389/fnhum.2015.00031.
109. Jonmohamadi, Y.; Forsyth A Fau - McMillan, R.; McMillan R Fau - Muthukumaraswamy, S.D.; Muthukumaraswamy, S.D. Constrained temporal parallel decomposition for EEG-fMRI fusion. *Journal of neural engineering* **2019**, *16,1*, doi:10.1088/1741-2552/aaefda.
110. Veer, I.M.; Beckmann Cf Fau - van Tol, M.-J.; van Tol Mj Fau - Ferrarini, L.; Ferrarini L Fau - Milles, J.; Milles J Fau - Veltman, D.J.; Veltman Dj Fau - Aleman, A.; Aleman A Fau - van Buchem, M.A.; van Buchem Ma Fau - van der Wee, N.J.; van der Wee Nj Fau - Rombouts, S.A.R.B.; Rombouts, S.A. Whole brain resting-state analysis reveals decreased functional connectivity in major depression. *Lasers in medical science* **2010**, *32,5*, 1153-1162, doi:10.1007/s10103-017-2221-y.
111. Shen, H.H. Core Concept: Resting-state connectivity. *Proceedings of the National Academy of Sciences of the United States of America* **2015**, *112, 46*, 14115-14116, doi:10.1073/pnas.1518785112.
112. Piano, C.; Imperatori, C.; Losurdo, A.; Bentivoglio, A.R.; Cortelli, P.; Della Marca, G. Sleep-related modifications of EEG connectivity in the sensory-motor networks in Huntington Disease: An eLORETA study and review of the literature. *Clinical neurophysiology : official journal of the International Federation of Clinical Neurophysiology* **2017**, *128,7*, 1354-1363, doi:10.1016/j.clinph.2016.11.019.
113. Jann, K.; Kottlow M Fau - Dierks, T.; Dierks T Fau - Boesch, C.; Boesch C Fau - Koenig, T.; Koenig, T. Topographic electrophysiological signatures of FMRI Resting State Networks. *PloS one* **2010**, *5,9* doi:10.1371/journal.pone.0012945.
114. Mohan, A.; Roberto, A.J.; Mohan, A.; Lorenzo, A.; Jones, K.; Carney, M.J.; Liogier-Weyback, L.; Hwang, S.; Lapidus, K.A. The Significance of the Default Mode Network (DMN) in Neurological and Neuropsychiatric Disorders: A Review. *The Yale journal of biology and medicine* **2016**, *89,1* 49-57.
115. Murphy, C.; Jefferies, E.; Rueschemeyer, S.A.; Sormaz, M.; Wang, H.T.; Margulies, D.S.; Smallwood, J. Distant from input: Evidence of regions within the default mode network supporting perceptually-decoupled and conceptually-guided cognition. *NeuroImage* **2018**, *171*, 393-401, doi:10.1016/j.neuroimage.2018.01.017.
116. Sormaz, M.A.-O.; Murphy, C.; Wang, H.T.; Hymers, M.; Karapanagiotidis, T.; Poerio, G.; Margulies, D.S.; Jefferies, E.; Smallwood, J. Default mode network can support the level of detail in experience during active

task states. *Proceedings of the National Academy of Sciences of the United States of America* **2018**, *115,37*, 9318-9323, doi:10.1073/pnas.1721259115.
117. Marek, S.; Dosenbach, N.U.F. The frontoparietal network: function, electrophysiology, and importance of individual precision mapping. *Dialogues in clinical neuroscience* **2018**, *20,2*, 133-140, doi:10.31887/DCNS.2018.20.2/smarek.
118. Vendetti, M.S.; Bunge, S.A. Evolutionary and developmental changes in the lateral frontoparietal network: a little goes a long way for higher-level cognition. *Neuron* **2014**, *84,5*, 906-917, doi:10.1016/j.neuron.2014.09.035.
119. Chan, R.C.; Shum D Fau - Toulopoulou, T.; Toulopoulou T Fau - Chen, E.Y.H.; Chen, E.Y. Assessment of executive functions: review of instruments and identification of critical issues. *Archives of clinical neuropsychology : the official journal of the National Academy of Neuropsychologists* **2008**, *23,2*, 201-216, doi:10.1016/j.acn.2007.08.010.
120. Collins, A.; Koechlin, E. Reasoning, learning, and creativity: frontal lobe function and human decision-making. *PLoS biology* **2012**, *10,3*, doi:10.1371/journal.pbio.1001293.
121. Kawasaki, M.; Kitajo K Fau - Yamaguchi, Y.; Yamaguchi, Y. Dynamic links between theta executive functions and alpha storage buffers in auditory and visual working memory. *The European journal of neuroscience* **2010**, *31,9*, 1683-1689, doi:10.1111/j.1460-9568.2010.07217.
122. Nielsen, J.D.; Madsen, K.H.; Wang, Z.; Liu, Z.; Friston, K.J.; Zhou, Y. Working Memory Modulation of Frontoparietal Network Connectivity in First-Episode Schizophrenia. *Cerebral cortex (New York, N.Y. : 1991)* **2017**, *27,7*, 3832-3841, doi:10.1093/cercor/bhx050.
123. Diamond, A. Executive functions. *Annual review of psychology* **2013**, *64*, 135-168, doi:10.1146/annurev-psych-113011-143750.
124. Hopfinger, J.B.; Slotnick, S.D. Attentional Control and Executive Function. *Cognitive neuroscience* **2020**, *11,1-2* 1-4, doi:10.1080/17588928.2019.1682985.
125. Binder, J.R.; Desai, R.H. The neurobiology of semantic memory. *Trends in cognitive sciences* **2011**, *15,11*, 527-536, doi:10.1016/j.tics.2011.10.001.
126. Tops, M.; Boksem, M.A. A potential role of the inferior frontal gyrus and anterior insula in cognitive control, brain rhythms, and event-related potentials. *Frontiers in psychology* **2011**, *2*, 330, doi:10.3389/fpsyg.2011.00330.
127. Grill-Spector, K.; Kourtzi Z Fau - Kanwisher, N.; Kanwisher, N. The lateral occipital complex and its role in object recognition. *Vision research* **2001**, *41,10-11* 1409-1422, doi:10.1016/s0042-6989(01)00073-6.
128. Cabeza, R.; Nyberg, L. Imaging cognition II: An empirical review of 275 PET and fMRI studies. *Journal of cognitive neuroscience* **2000**, *12,1*, 1-47, doi:10.1162/08989290051137585.
129. Bisley, J.W.; Goldberg, M.E. Neuronal activity in the lateral intraparietal area and spatial attention. *Science (New York, N.Y.)* **2003**, *299,5603*, 81-86, doi:10.1126/science.1077395.
130. Posner Mi Fau - Walker, J.A.; Walker Ja Fau - Friedrich, F.J.; Friedrich Fj Fau - Rafal, R.D.; Rafal, R.D. Effects of parietal injury on covert orienting of attention. *The Journal of neuroscience : the official journal of the Society for Neuroscience* **1984**, *4,7*, 1863-1874, doi:10.1523/JNEUROSCI.04-07-01863.1984.
131. Kamiński, J.; Brzezicka A Fau - Gola, M.; Gola M Fau - Wróbel, A.; Wróbel, A. β band oscillations engagement in human alertness process. *International journal of psychophysiology : official journal of the International Organization of Psychophysiology* **2012**, *85,1*, 125-128, doi:10.1016/j.ijpsycho.2011.11.006.
132. Gross, J.; Schmitz F Fau - Schnitzler, I.; Schnitzler I Fau - Kessler, K.; Kessler K Fau - Shapiro, K.; Shapiro K Fau - Hommel, B.; Hommel B Fau - Schnitzler, A.; Schnitzler, A. Modulation of long-range neural synchrony reflects temporal limitations of visual attention in humans. *Proceedings of the National Academy of Sciences of the United States of America* **2004**, *101,35*, 13050-13055, doi:10.1073/pnas.0404944101.